

Tubular Structure Segmentation based on Heat Diffusion

Fang Yang and Laurent D.Cohen

University Paris Dauphine, PSL Research University, CNRS, UMR 7534,
CEREMADE, 75016 PARIS, FRANCE

Abstract. This paper proposes an interactive method for tubular structure segmentation. The method is based on the minimal paths obtained from the geodesic distance solved by heat equation. This distance can be based both on isotropic or anisotropic metric by solving the corresponding heat equation. Thanks to the additional dimension added for the local radius around the centerline, our method can not only detect the centerline of the structure, but also extracts the boundaries of the structures. Our algorithm is tested on both synthetic and real images. The promising results demonstrate the robustness and effectiveness of the algorithm.

1 Introduction

In computer vision field, it is significant to obtain geodesic distance and geodesic lines. They play a very important role in road extraction, vessel segmentation, surface re-meshing and so on [14]. In general, the geodesic distance ϕ could be acquired via Dijkstra's method [5] or solving the Eikonal equation $\|\nabla\phi\| = \mathcal{P}$, where \mathcal{P} is a potential cost function computed from the image I . The Fast Sweeping Method [22] and the Fast Marching Method [16, 3] are quite often used to solve the Eikonal equation. For the extraction of the geodesic lines γ^* between the initial point p_{s_0} and the endpoint p_x , it can be achieved by solving an ordinary differential equation after the computation of ϕ :

$$\forall s > 0, \frac{d\gamma^*}{ds} = -\frac{\nabla\phi}{\|\nabla\phi\|}, \gamma^*(0) = p_x \quad (1)$$

The heat equation is a partial differential equation (PDE) that describes the evolution of the distribution of heat on a domain within time T . It has a general form:

$$\frac{\partial u}{\partial t} = \alpha \Delta u \quad (2)$$

where u stands for the heat, and α , a positive constant, represents the thermal conductivity, Δ is the Laplace operator.

In 1967, Varadhan [18] proposed a formula to approximate the geodesic distance $\phi(p_0, p_x)$ between two points p_0 and p_x on a Riemannian manifold:

$$\phi(p_0, p_x) = \lim_{t \rightarrow 0} \sqrt{-4t \log u_{p_0}(p_x, t)} \quad (3)$$

where u_{p_0} the solution of Eq.(2) under the initial condition that $u_{p_0}(0) = \delta_{p_0}$ within a small time $t \rightarrow 0$.

Recently, Crane *et al.*[4] proposed a heat method to estimate the geodesic distance. Their approach can be divided into three steps: (1) solve Eq.(2) for some fixed time t ; (2) normalize the vector field: $X = -\nabla u/|\nabla u|$; (3) solve the Poisson equation to obtain the geodesic distance: $\Delta\phi = \nabla \cdot X$. By comparing the heat method with the state-of-the-art Fast Marching Method [16], Crane *et al.* found that, using the heat method to obtain the geodesic distance is faster than the Fast Marching Method. This is due to the fact that steps (1) and (3) can be pre-factorized. Furthermore, the authors used a direct solver to solve the heat equation. In [15, ?], the authors proves that the sparse systems arising from the elliptic PDEs can be solved in very close to linear time.

More recently, Yang and Cohen [21] have extended and gone beyond the work of Crane *et al.*. They introduced isotropic and anisotropic heat flows to approximate the geodesic distance by using Varadhan’s formula Eq.(3). Then they use an ordinary differential equation (ODE) for backtracking the minimal path γ^* , for the isotropic case, they use Eq.(1), and for the anisotropic case, they use:

$$\forall s > 0, \frac{d\gamma^*}{ds} = -\frac{D^{-1}\nabla\phi}{\|D^{-1}\nabla\phi\|}, \gamma^*(0) = p_x \quad (4)$$

where D is the metric tensor. It is shown in [21] that using the heat method to approximate the geodesic distance is not only fast and efficient, but also less sensitive to noise.

In the past few decades, numerous segmentation method based on minimal paths have been proposed, such as [3, 10, 1, 2, 21].

In [21], the authors use different heat flows to obtain the geodesic distance and geodesic lines, they could only extract the centerlines of the structures, but not able to extract the boundaries at the same time. While in [10], instead of using the pure spatial traditional minimal path technique [3], Li and Yezzi have incorporated an additional non-spatial dimension, which can be used to measure the thickness (radius) of the structures in space. In other words, this additional dimension can help to extract the boundaries and surfaces of the structures in 2D and 3D spaces. And in the meantime, their method can also detect a precise centerline of the structures. But the potential \mathcal{P} that is used in [10] is isotropic and depends on the positions. The orientations of the tubular structures are ignored. Later on, Benmansour *et al.*[1] have proposed an anisotropic minimal path model which also takes the additional dimension into account, so the potential depends both on the positions and the tangent directions. The way they built the metric was based on the anisotropic Optimally Oriented Flux (OOF) descriptor proposed by Law and Chung [9]. The OOF descriptor makes the propagation faster along the tubular structures. The advantage of the anisotropic model lies in that it can avoid the shortcut issues effectively. Then Benmansour and Cohen have extended their method into 3D vessel extraction [2].

Despite that in [10, 2], the authors use the Fast Marching Method to get the numerical solution of the Eikonal equation, in this paper, we are interested in

the segmentation of tubular structures by using the heat method. Here, we use the same way to construct metric tensor as the authors do in [1, 2]. This is called $2D + Radius$ model in heat. To solve the heat equation, we use the backward scheme.

The contribution of this work is that we add a non-spatial third dimension in both isotropic and anisotropic heat diffusion to segment tubular structures. We use the OOF descriptor [9] to build the metric. Therefore, the heat method can be used to detect the centerlines and boundaries simultaneously.

This paper is organized as follows: in Sect-2, we give some background on the minimal path, the heat diffusion, and the OOF descriptor; in Sect-3, how to construct the metric and the way to solve the heat equation are presented; in Sect-4, we test our method on some synthetic and real data. Sect-5 provides some concluding remarks and possible directions for future work.

2 Background

2.1 Minimal Paths

Given an image $I : \Omega \rightarrow \mathbb{R}^2$ and two points p_{s_0} and p_x , the geodesic γ is a curve connecting these two points that globally minimizes the following energy functional $E : \mathcal{A}_{p_{s_0}, p_x} \rightarrow \mathbb{R}^+$:

$$E(y(s)) = \int_{\Omega} \{\mathcal{P}(y(s)) + w\} ds, \quad y(s) \in \mathcal{A}_{p_0, p_x} \quad (5)$$

where \mathcal{P} is a potential cost function computed from I , w is a positive constant that imposes regularity on the curve. $\mathcal{A}_{p_{s_0}, p_x}(s)$ is the set of all the curves linking p_{s_0} and p_x , s is the arclength.

To solve this minimalization problem, Cohen and Kimmel [3] proposed a Hamiltonian approach: Find the minimal action map $\phi : \Omega \rightarrow \mathbb{R}^2$ that solves the Eikonal equation:

$$\|\nabla\phi\| = \mathcal{P} + w \quad (6)$$

with the boundary condition $\phi(p_{s_0}) = 0$. Popular ways to solve the Eikonal equation such as the Fast Marching [16, 3] and Fast Sweeping [22] are quite often used. But these methods do not reuse information [4]: once the geodesic distance ϕ_{s_0} from the initial source point p_{s_0} is obtained, the distance from another source point p_{s_1} needs to be recomputed from scratch. According to Eq.(3), ϕ can be also approximated by the heat kernel. The advantage of using the heat kernel is that the Laplace operator could be precomputed, so that the fundamental solution of the heat equation can be acquired in a single step no matter where the initial point p_{s_0} is. In this way, the approximation of ϕ can be obtained once the heat equation is solved. Then the geodesic γ could be obtained by solving Eq.(1) or Eq.(4) depending on the heat diffusion being isotropic or anisotropic.

2.2 Isotropic and Anisotropic Heat Diffusion

Eq.(2) presents a homogeneous form of heat equation. When it comes to isotropic and anisotropic heat diffusion, the heat equation could be written as:

$$\frac{\partial u}{\partial t} = k \operatorname{div} \cdot (D \nabla u) \quad (7)$$

where k is the diffusivity, it can be a constant (as α in Eq.(2)) or a scalar function, and D can be a scalar function or a diffusion tensor. According to [19], when D is a scalar function, the heat diffusion is isotropic. And when D is a diffusion tensor, it is a tensor field of symmetric positive matrices that can encode the local orientation and anisotropy of an image [21]. Then the heat diffusion becomes anisotropic. For the 2D heat diffusion, the tensor field D can be decomposed as shown in Eq.(8):

$$D = \lambda_1 \mathbf{e}_1 \mathbf{e}_1^T + \lambda_2 \mathbf{e}_2 \mathbf{e}_2^T \quad (8)$$

λ_1 and λ_2 are the eigenvalues, $\lambda_2 \geq \lambda_1 \geq 0$, \mathbf{e}_1 and \mathbf{e}_2 are the the corresponding orthogonal eigenvectors. A measure of the local anisotropy can be defined as $A = (\lambda_2 - \lambda_1)/(\lambda_2 + \lambda_1)$. When $\lambda_1 = \lambda_2$, the heat diffusion becomes isotropic.

The main difference between isotropic and anisotropic diffusion lies in the fact that isotropic diffusion does not include the local orientation, while using the anisotropic diffusion, heat could be more concentrated on the directions that the users design.

2.3 Optimally Oriented Flux

In order to use the relevant anisotropic heat equation, we need to find some estimates for the local orientation and scale to describe the tube-like structures. In fact, many classical enhancers like the Hessian-based vesselness measures have been proposed [8, 11]. But the Hessian-based enhancers include adjacent features. While the OOF descriptor [9] avoids this problem.

Given an image $I : \Omega \rightarrow \mathbb{R}^2$, the oriented flux is the amount of the image gradient projected along the axis \mathbf{p} flowing out from a 2D circle \mathcal{S}_r at point \mathbf{x} with radius r :

$$f(\mathbf{x}; r, \mathbf{p}) = \int_{\partial \mathcal{S}_r} (\nabla(G_\sigma * I)(\mathbf{x} + r\mathbf{n}) \cdot \mathbf{p})(\mathbf{p} \cdot \mathbf{n}) ds \quad (9)$$

where G_σ is a Gaussian with some variance σ , and empirically σ is set to 1. \mathbf{n} is the outward unit normal of $\partial \mathcal{S}_r$. ds is the infinitesimal length on $\partial \mathcal{S}_r$. Based on the divergence theorem, the oriented flux $f(\mathbf{x}, r; \mathbf{p}) = \mathbf{p}^T \mathbf{Q}_{r, \mathbf{x}} \mathbf{p}$, where $\mathbf{Q}_{r, \mathbf{x}}$ is a symmetric matrix.

In [9], the authors used only the eigenvalues λ_i of $\mathbf{Q}_{\mathbf{x}, r}$ for the vessel enhancement. While in this paper, we use both the eigenvalues λ_i and the eigenvectors \mathbf{e}_i to form the diffusion tensor, thus the heat could be more concentrated on the tube-like structures.

3 Construction of the Metric and Numerical Solutions of the Heat Equation

3.1 Construction of the Metric

Now we are considering building a $(d + 1)$ D metric, d is the dimension of the image, in our case, $d = 2$, and the 3rd dimension is not spatial but a radius dimension. We use the same way as described in [2] to construct the metric.

$$D(x, r) = \begin{bmatrix} \hat{D}(x, r) & \mathbf{0} \\ \mathbf{0} & \mathcal{P}_r(x, r) \end{bmatrix} \quad (10)$$

where $\hat{D}(x, r)$ is a 2×2 symmetric matrix, this entry is used to describe the spatial anisotropy. In addition, $\mathcal{P}_r(x, r)$ is the isotropic radius potential entry. For a certain scale r , the anisotropic entry \hat{D} can be constructed by the eigenvalues λ_i ($i \in 1, 2$) ($\lambda_2 > \lambda_1$) and the eigenvectors \mathbf{v}_i of the OOF descriptor:

$$\hat{D}(x, r) = \eta_1 (\exp(\beta \cdot \lambda_1(x)) \mathbf{v}_1(x) \mathbf{v}_1(x)^T + \exp(\beta \cdot \lambda_2(x)) \mathbf{v}_2(x) \mathbf{v}_2(x)^T) \quad (11)$$

The radius potential entry can be described by the eigenvalues of the OOF descriptor.

$$\mathcal{P}_r(x) = \eta_2 \exp\left(\beta \frac{\lambda_1(x) + \lambda_2(x)}{2}\right) \quad (12)$$

Here β is a constant that is controlled by the maximal spatial anisotropic ratio μ , which is defined as:

$$\mu = \max_{x, r} \sqrt{\exp(\beta \cdot (\lambda_2(x, r) - \lambda_1(x, r)))} \quad (13)$$

By choosing the maximal spatial anisotropy ratio μ , β is then fixed. $0 \leq \eta_1, \eta_2 \leq 1$ are two constants that control the space and radius speed. If we would like the heat to propagate faster on the radius dimension, we could choose a bigger $\eta_2 > \eta_1$. In this paper, η_1 and η_2 are always set to be 1. Using Eq.(10) as the diffusion tensor in Eq.(7), the heat equation can be written as:

$$\frac{\partial u(x, r, t)}{\partial t} = \text{div} \cdot (D(x, r) \nabla u(x, r, t)) \quad (14)$$

For the isotropic diffusion, the metric D becomes:

$$D(x, r) = \mathcal{P}_r(x, r) I_d \quad (15)$$

I_d is an 3×3 identity matrix.

3.2 Solving the Heat Equation

After the construction of the metric, we now solve the heat equation. Generally, the numerical approximation to the solution of the discrete heat equation could be achieved by different schemes [13, 6, 20, 7].

Given the image $I : \Omega \rightarrow \mathbb{R}^2$, suppose that the domain of is discretized into $M \times N$ grids and the scale of the third dimension $r \in [R_{min}, R_{max}]$ is K.

Then the initial heat value $u^0 = [u_{1,1,1}^0, u_{1,2,1}^0, \dots, u_{1,N,1}^0, u_{2,1,1}^0, u_{2,2,1}^0, \dots, u_{2,N,1}^0, \dots, u_{N,N,M}^0]$, with $u_{i',j',k'}^0 = 1$ for all $(i', j', k') \neq (i, j, k)$ is the initial point given by the users.

Numerical Solution of Isotropic Diffusion For the isotropic diffusion, we use a backward finite differences scheme, which is also called implicit finite differences scheme. Take the 3D heat equation Eq.(2) into consideration, the backward finite difference scheme would be:

$$(\text{Id} - \tau\alpha\Delta)u^t = u^0 \quad (16)$$

Id is the identity matrix, τ is the diffusion time, u^t is the heat value after time τ . The Laplace operator Δ can be easily discretized as an $N^2 \times M \times N^2 \times M$ block penta-diagonal sparse matrix. After the discretization of the Laplace operator Δ , the heat distribution u^t can be acquired by setting an appropriate time step τ .

Numerical Solution of Anisotropic Diffusion For the anisotropic diffusion, we use a backward discretization scheme designed by Fehrenbach and Mirebeau [7]. The scheme is called Anisotropic Diffusion using Lattice Basis Reduction (AD-LBR). The advantages of this scheme are its non-negativity and sparsity, thus making the solution robust and fast.

For Eq.(14), the backward scheme is:

$$\frac{u^t - u^0}{\tau} = \text{div} \cdot (D\nabla u^t) \quad (17)$$

To acquire the fundamental solution of Eq.(17) within a small time τ , we have:

$$(\text{Id} - \tau \text{div} \cdot (D\nabla))u^t = u^0 \quad (18)$$

The symmetric operator $A = \text{div} \cdot (D\nabla)$, with Neumann boundary conditions, can also be defined through the identity

$$\int_{\Omega} u(x) Au(x) dx = \int_{\Omega} \nabla u(x)^T D(x) \nabla u(x) dx, \quad (19)$$

for all $u \in H^1(\Omega)$. In order to discretize A , the AD-LBR approximates the contribution of each grid point $x \in \Omega$ to the r.h.s. of (19) using a sum of squared finite differences

$$\nabla u(x)^T D(x) \nabla u(x) \approx \sum_{v \in V(x)} \omega_x(v) \left(\frac{u(x + hv) - u(x)}{h} \right)^2, \quad (20)$$

where $h > 0$ is the grid scale, $V(x)$ is a set of vectors referred to as the *stencil* of the point x , and $\omega_x(v)$ is the *weight* of the vector v at x . From these stencils

and weights, the sparse symmetric matrix of A is then easily assembled. The specificity of the AD-LBR numerical scheme is that the stencils are sparse, with at most 12 elements in 3D, which limits the numerical cost of the method, and that the weights are non-negative, which guarantees discrete maximum principle as well as the robustness of the method.

Their computation involves the construction at each grid point $x \in \Omega$ of an obtuse superbase with respect to the matrix $D(x)$, which is a family $(e_i)_{i=0}^d$ of vectors with integer coordinates such that $|\det(e_1, \dots, e_d)| = 1$ and $e_i^T D(x) e_j \leq 0$ for all $0 \leq i < j \leq d$. The stencil is then $V(x) = \{e_i \times e_j; i \neq j\}$ and the corresponding non-negative weights are $\omega_x(e_i \times e_j) = -\frac{1}{2} e_k^T D(x) e_l$ whenever (i, j, k, l) are pairwise distinct, $i, j, k, l \in \{0, 1, 2, 3\}$. The stencil construction is cheap and efficient thanks to arithmetic techniques, thus computation time is dominated by solving the linear systems. See [7] for details.

4 Experiments and Results

4.1 Experiment Data and Settings

We have tested our method both on synthetic and real images:

Fig.1 is an example on a noisy synthetic image (a) of size 100×100 . This image is obtained by corrupting the original image with 35% pepper & salt noise. The ground truth in (d) is the original image without adding the noise. The blue curve stands for the center line and the red contour represents the boundary of the tubular structure. Fig.2a is a 300×300 vessel image and Fig.2d is a 200×160 road image.

In Fig.3, to illustrate the advantage of anisotropic diffusion, we use a 100×100 image with a tube-like structure which has sharp corners.

Fig.4a demonstrates a medical image with a catheter. And before diffusion, to preprocess the image I , we first build a potential \mathcal{P} based on the image Laplacian, then we use a sigmoid function Eq.(21) on \mathcal{P} .

$$I_m(x) = 1 - \frac{1}{1 + e^{\lambda(\mathcal{P}(x) - k)}} \quad (21)$$

I_m is the result after preprocessing. Here we set $\lambda = 10$ and $k = 0.5$.

For all the experiment results, the red points and blue points represent the initial points and endpoints respectively. We use the red curves to segment the structures boundary. And the blue curves stand for the centerlines. For the first three experiments, the same diffusion time $\tau = 0.01$ is employed.

To evaluate the performance of our method, we make some comparisons with the state-of-the-art Fast Marching Method. In addition, we compute the *precision* and *recall*:

$$\begin{cases} recall = \frac{TP}{TP+FN} \\ precision = \frac{TP}{TP+FP} \end{cases} \quad (22)$$

Here TP represents the segmentation part which matches the ground truth (GT), FP is the part that do not coincide the GT, FN stands for the part that are missing extracted.

4.2 Results and Analysis

Isotropic Diffusion on a Noisy Synthetic Image Fig.1 is an example on a noisy synthetic image (a), with a percentage 0.35 of corrupted pixels. (d) is the ground-truth obtained by using the Fast Marching Method on the image without adding noise. From the two results (e) and (f), compared with the ground-truth (d), we can see that the heat method outperforms the Fast Marching Method, because not only the centerline but also the boundaries extracted by heat method are smoother than the ones extracted by the Fast Marching Method. Table-1 presents the *precision* and *recall* and the corresponding time consumption of these two methods. It turns out that the heat method does better than the Fast Marching Method. Additionally, the distance map obtained by Fast Marching (b) is more noisy then the one by heat diffusion (c). The distance maps (b) and (c) illustrate that the heat method is very robust in noisy circumstances. This is due to the fact that the heat equation can get fast smoothing by nature. With the initial condition $u(x_0, y_0, t_0) = \delta_{x_0, y_0}(t_0)$, the heat becomes smooth as soon as $t > t_0$. Additionally, in the sense of mathematics, the solutions of the heat equation are characterized by a Gaussian kernel, this can be regarded as a blurring process. This is also the reason that heat method can be used for filtering issues.

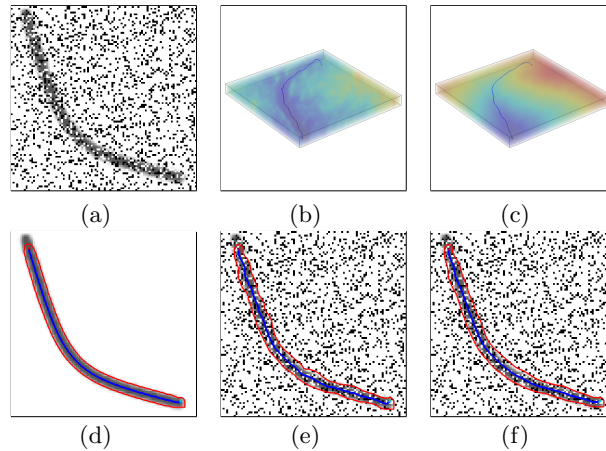


Fig. 1. Experiment on a noisy image: (a) original noisy image; (b) and (c) are the distance maps ϕ and the 3D minimal path between the seed point and endpoint (transparent visualization) by using the isotropic Fast Marching Method and isotropic Heat Method. (d) is the ground-truth; (e) and (f) are the results by the Fast Marching Method and Heat Method.

Isotropic Diffusion on a Vessel Image and a Road Image Fig.2 demonstrates the experiments on a vessel image and a road image. We are using the

Table 1. time consumption and the indexes of evaluation%.

data	heat method				fast marching method		
	precompute	solve	precision	recall	time	precision	recall
noisy curve	0.06s	0.06s	94.24	97.58	0.16s	92.97	93.54
vessel	0.745s	1.05s	89.54	90.31	1.846s	91.26	88.62
road	0.2s	0.32s	93.40	99.82	0.63s	92.51	97.91

same isotropic metric for the Fast Marching Method and the heat method. For the vessel image (a), one initial points and several endpoints are selected manually. From Table-1, we can see the result by the heat method is comparable with the Fast Marching Method. For the road image (d), there are many abandoned cars on both sides of the road, which may cause much influence in boundary detection. From the results (e) and (f), we can see that the accuracy of the boundaries (highlighted in the green rectangles) that extracted by our method is higher than Fast Marching. In other words, our result is less influenced by the cars than Fast Marching. In addition, our method gives a smoother result than Fast Marching.

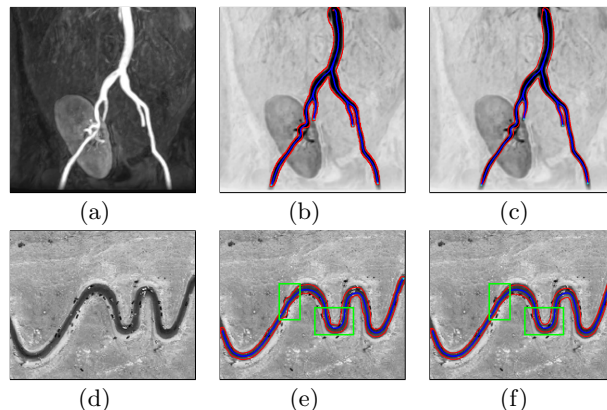


Fig. 2. Example on a medical image with several endpoints (row above) and on a road image (row below), from left to right, they are the original images, the result by the Fast Marching Method and the result by the heat method. The green rectangles illustrate the places that the heat method surpasses the Fast Marching Method.

Isotropic and Anisotropic Diffusion on a Tube-like Structure In Fig-3, there is a tube-like structure with several sharp corners. Here we test the difference between isotropic and anisotropic methods. From (b), it is obvious that there is a short-cut on the way back to the initial points, while in (c), the backtracking process is totally along the structure without any short-cut. This

indicates that by using the anisotropic heat diffusion, the heat can be more concentrated on the direction that the users design.

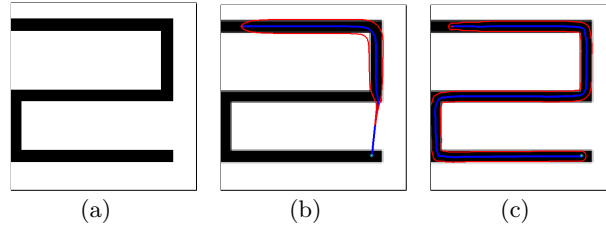


Fig. 3. Example on a tube-like structure image, (a) the original image, (b) the result by the isotropic heat method, (c) the result by the anisotropic heat method. There is a short-cut of (b) while in (c), the detection result is along the structure without short-cut.

Diffusion on a Medical Image within different time step The time step τ is an important factor for the heat method. It decides the time for diffusion. According to Eq.(3), the distance map ϕ could be approximated only when the diffusion time t is as small as possible. Fig.4 demonstrates the effect of diffusion time τ . Different τ are applied. From (b) to (d), τ equals to 0.1, 0.01 and 0.001 respectively. From the results, it can be seen clearly that the longer the diffusion time is, the more the distance map gets blurred, thus leading to the shortcut on the way when backtracking to the initial point.

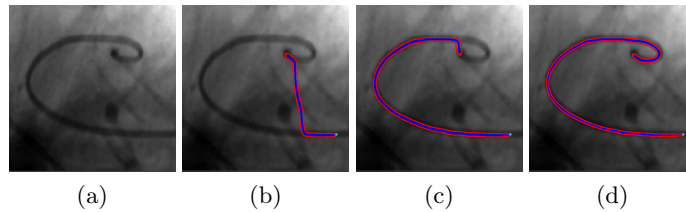


Fig. 4. Experiment on a real medical image: (a) original image; (b) (c) (d) are the results generated by isotropic heat diffusion with different time step τ .

5 Conclusion and Prospects

We have proposed a $2D + Radius$ model in heat diffusion to extract the center-lines as well as the boundaries of the tubular structures in 2D images. This model integrate the OOF descriptor and diffusion tensor. From the results, we can see that the $2D + Radius$ model in heat is very robust and efficient. Compared with

the Fast Marching Method, it has a strong anti-noise performance. In addition, the anisotropic diffusion does better in controlling the direction than isotropic diffusion. It is fit for detecting the very curved lines and structures.

In future, we are interested in extending this model to higher dimension. We also would like to propose some automatic methods based on this model, in this way, we no longer need to provide the end points, which could save a lot of human interventions.

References

1. Benmansour, Fethallah and Cohen, Laurent D. and Law, Max and Chung, Albert: Tubular anisotropy for 2D vessel segmentation. IEEE Conference on Computer Vision and Pattern Recognition, 2009. CVPR 2009.
2. Benmansour, Fethallah and Cohen, Laurent D.: Tubular structure segmentation based on minimal path method and anisotropic enhancement. International Journal of Computer Vision. 92, 192–210(2011)
3. Cohen, Laurent D. and Kimmel, Ron: Global minimum for active contour models: A minimal path approach. International Journal of Computer Vision. 24, 57–78(1997)
4. Crane, Keenan and Weischedel, Clarisse and Wardetzky, Max: Geodesics in heat: A new approach to computing distance based on heat flow. ACM Transactions on Graphics (TOG). 32, 152(2013)
5. Dijkstra, Edsger W.: A note on two problems in connexion with graphs. Numerische mathematik. 1, 269–271(1959)
6. Douglas, Jim and Rachford, Henry H.: On the numerical solution of heat conduction problems in two and three space variables. Transactions of the American mathematical Society. 82,421–439(1956)
7. Fehrenbach, Jérôme and Mirebeau, Jean-Marie: Sparse non-negative stencils for anisotropic diffusion. Journal of Mathematical Imaging and Vision. 49,123–147(2014)
8. Frangi, Alejandro F. and Niessen, Wiro J. and Vincken, Koen L. and Viergever, Max A.: Multiscale vessel enhancement filtering. Medical Image Computing and Computer-Assisted Intervention MICCAI 98 (1998)
9. Law, Max WK and Chung, Albert CS: Three dimensional curvilinear structure detection using optimally oriented flux. European Conference on Computer Vision–ECCV 2008
10. Li, Hua and Yezzi, Anthony: Vessels as 4-D curves: Global minimal 4-D paths to extract 3-D tubular surfaces and centerlines. IEEE Transactions on Medical Imaging. 26, 1213–1223 (2007)
11. Lindeberg, Tony: Edge detection and ridge detection with automatic scale selection. International Journal of Computer Vision. 30, 117–156 (1998)
12. Mirebeau, Jean-Marie and Fehrenbach, Jérôme and Risser, Laurent and Tobji, Shaza: Anisotropic Diffusion in ITK. The Insight Journal.(2015)
13. Peaceman, Donald W. and Rachford, Jr, Henry H.: The numerical solution of parabolic and elliptic differential equations. Journal of the Society for industrial and Applied Mathematics. 3, 28–41, (1955)
14. Peyré, Gabriel and Péchaud, Mickaël and Keriven, Renaud and Cohen, Laurent D.: Geodesic methods in computer vision and graphics. Foundations and Trends® in Computer Graphics and Vision. 5, 197–397, (2010)

15. Schmitz, Phillip G and Ying, Lexing.: A fast direct solver for elliptic problems on general meshes in 2D. *Journal of Computational Physics*. 231, 1314–1338, (2012)
16. Sethian, James A.: A fast marching level set method for monotonically advancing fronts. *Proceedings of the National Academy of Sciences*. 93, 1591–1595, (1996)
17. Spielman, Daniel A. and Teng, Shang-Hua.: Nearly-linear time algorithms for graph partitioning, graph sparsification, and solving linear systems. *Proceedings of the thirty-sixth annual ACM symposium on Theory of computing*. (2004)
18. Varadhan, Sathamangalam R. Srinivasa.: On the behavior of the fundamental solution of the heat equation with variable coefficients. *Communications on Pure and Applied Mathematics*. 20, 431–455 (1967)
19. Weickert, Joachim.: *Anisotropic diffusion in image processing*. Teubner Stuttgart. (1998)
20. Weickert, Joachim and Scharr, Hanno.: A scheme for coherence-enhancing diffusion filtering with optimized rotation invariance. *Journal of Visual Communication and Image Representation*. 13, 103–118, (2002)
21. Yang, Fang and Cohen, Laurent D.: Geodesic Distance and Curves Through Isotropic and Anisotropic Heat Equations on Images and Surfaces. *Journal of Mathematical Imaging and Vision*, 55(2): 210-228, (2016)
22. Zhao, Hongkai: A fast sweeping method for eikonal equations. *Mathematics of computation*, 74: 603–627, (2005)